Supplementary Material

Development of PdO/ $Sr_3Fe_2O_{7-\delta}$ /*a*-Al_2O_3 catalysts for methane combustion

Yeon-Bin Choi[a,†,#], Tae Wook Kang[a,#], Seo Young Kim[a], Seon Tae Kim[a], Byung seo Bae[b], Do yun Kim[c,*], Jin-Su Kwak[c,*], and Sun Woog Kim[a,*]

[a]Electronic Convergence Materials Division, Optic & Electronic Component Materials Center, Korea Institute of Ceramic Engineering and Technology, Jinju 52851, Republic of Korea

[b]Advanced Resources Team, Yeongwol Industrial Promotion Agency, 21–28 Palgoe 1 Nonggongdanji, Yeongwolgun 26240, Republic of Korea

[c]Korea Shipbuilding & Offshore Engineering Co., Ltd., Seoul 03058, Republic of Korea

[†]current address: Advanced Resources Team, Yeongwol Industrial Promotion Agency, 21–28 Palgoe 1 Nonggongdanji, Yeongwolgun 26240, Republic of Korea

Calculation of turnover frequency (TOF) and specific reaction rate

The first order rate constants, k (in h^{-1}), were calculated by monitoring the combustion of CH_4. A linear plot using the following equation was used to determine k :[58]

$$\ln\left(\frac{n0,CH4}{nt,CH4}\right) = k \cdot t \quad (1)$$

where $n_{0,CH4}$ is initial amount of CH_4 (in mmol), $n_{t,CH4}$ is amount of CH_4 (in mmol) at reaction time, t (in h), and t is reaction time (in h). In addition, the specific reaction rate for the methane conversion reaction were calculated using the pseudo first-order reaction model : [52]

$$r = k \cdot C \quad (2)$$

where *r* is the reaction rate, k is the apparent rate constant, and *C* is the methane concentration. The catalytic conversion activity was evaluated using the specific reaction rate expressed per mass unit of catalyst ($mmol \cdot s^{-1} \cdot g^{-1}$) at a reaction temperature of 275 °C.

Surface PdO density, ρ_{PdO}(in sites/m^2), was calculated according to :[58]

$$\rho_{PdO} = \frac{nPdO \cdot NA}{mNDIR \cdot SAcat} \quad (3)$$

where n_{PdO} is the moles of surface PdO sites in each sample, N_A is Avogadro's number, m_{NDIR} is the mass loading of catalysts (in g) used in a non-dispersive infrared (NDIR) gas analyzer, and SAcat is surface area of catalysts (in m^2/g).

The turnover frequency (TOF, in h^{-1}) for each catalysts corresponding to PdO loading amount at 225 °C was calculated by taking the ratio of the CH_4 combustion rate over the density of surface PdO active sites :[58]

$$TOF = \frac{k \cdot nf,CH4 \cdot NA}{\rho PdO} \quad (4)$$

where $n_{f, CH4}$ is amount of CH_4 combustion after reaction.

Surface oxygen vacancy density (ρ_{Vo}) estimated based on the amount of ad-O_2 derived from the O_2-TPD analysis and TOF over the density of surface oxygen vacancy density are calculated as follow.

Surface oxygen vacancy density, ρ_{Vo} (in sites/m^2), was calculated according to : [58]

$$\rho_{Vo} = \frac{nVo \cdot NA}{mNDIR \cdot SAcat} \quad (5)$$

where n_{Vo} is the moles of surface oxygen vacancy sites in each sample, N_A is Avogadro's number, m_{NDIR} is the mass loading of catalysts (in g) used in a non-dispersive infrared (NDIR) gas analyzer, and SAcat is surface area of catalysts (in m^2/g).

The turnover frequency (TOF, in h^{-1}) for each catalysts corresponding to surface oxygen vacancy density at 275 °C was calculated by taking the ratio of the CH_4 combustion rate over the density of surface oxygen vacancy :[58]

$$TOF = \frac{k \cdot nf,CH4 \cdot NA}{\rho VO} \quad (6)$$

Table S1. Summary of various catalysts and reaction conditions for methane oxidation in fixed-bed reactor.

Catalyst	Surface area (m^2/g)	Reactant	$T_{50\%}$ (℃)	$T_{90\%}$ (℃)	Ref.
0wt%Pd/$LaMnO_3 \cdot 2ZrO_2$	29.82	CH_4: 2vol%, O_2: 4vol%, N_2: balance, GHSV: 48,000h^{-1}	520	-	59
0.5wt%Pd/$LaMnO_3 \cdot 2ZrO_2$	28.88		509	-	
1wt%Pd/$LaMnO_3 \cdot 2ZrO_2$	29.30		485	-	
2wt%Pd/$LaMnO_3 \cdot 2ZrO_2$	28.64		432	-	
3wt%Pd/$LaMnO_3 \cdot 2ZrO_2$	27.43		461	-	
0.5wt%Pd/$La_2Zr_2O_7$	-		531	-	
1wt%Pd/$La_2Zr_2O_7$	-		518	-	
2wt%Pd/$La_2Zr_2O_7$	-		476	-	
3wt%Pd/$La_2Zr_2O_7$	-		498	-	
3DOM;$La_{0.6}Sr_{0.4}MnO_3$	32.4	CH_4: 5vol%, O_2: 30vol%, Ar: balance, GHSV: 50,000h^{-1}	384	508	60
1wt%Pd/3DOM;$La_{0.6}Sr_{0.4}MnO_3$	32.0		358	378	
2wt%Pd/Al_2O_3	334	CH_4: 1vol% in Air, GHSV: 5,800h^{-1}	367	497	61
2wt%Pd/Al_2O_3-$ZrSiO_4$	217		360	415	
2wt%Pd/Al_2O_3-SiO_2	356		360	447	
0.5wt%Pd/3CeO_2/Al_2O_3	680	CH_4: 1vol% in Air, GHSV: 5,800h^{-1}	648	-	62
0.5wt%Pd/5CeO_2/Al_2O_3	343		623	-	
0.5wt%Pd/3La_2O_3/Al_2O_3	369		705	-	
0.5wt%Pd/5La_2O_3/Al_2O_3	650		723	-	
2wt%Pd/CeO_2	53.6	CH_4: 1vol% in Air, GHSV: 50,000h^{-1}	557	-	63

Table S1 (continued)

Catalyst	Surface area (m^2/g)	Reactant	$T_{50\%}$ (°C)	$T_{90\%}$ (°C)	Ref.
1wt%Pd/HZSM-5	498.1		351	-	
1wt%Pd-Ce/HZSM-5	493.5		336	-	
1wt%Pd-La/HZSM-5	438.4	CH_4: 2vol%, O_2: 8vol%, N_2: balance, GHSV: 48,000h^{-1}	387	-	64
1wt%Pd-Sm/HZSM-5	455.0		374	-	
1wt%Pd-Nd/HZSM-5	462.2		371	-	
1wt%Pd-Tb/HZSM-5	419.1		388	-	
2wt%Pd/CeO_2·2ZrO_2	74.6		382	429	
2wt%Pd/$LaMnO_3$·2ZrO_2	132.5	CH_4: 2vol%, O_2: 16vol%, He: balance	570	645	65
2wt%Pd/$BaCeO_3$·2ZrO_2	26.4		512	592	
4wt%PdO/meso-$Ce_{0.2}Zr_{0.35}Y_{0.05}O_2$	120.1	CH_4: 2.5vol%, GHSV: 50,000h^{-1}	320	360	66
2.94wt%Pd/meso-Co_3O_4	108.1	CH_4: 2.5vol%, GHSV: 20,000h^{-1}	288	334	67
1.41wt%Pd/meso-Mn_2O_3	89.9	CH_4: 2.5vol%, GHSV: 20,000h^{-1}	380	460	68
0.97wt%Pd/3DOM;$LaMnAl_{11}O_{19}$	28.8	CH_4: 2.5vol%, GHSV: 20,000h^{-1}	308	343	69
1.87wt%Pd/MnO_x/3DOM;$CoFe_2O_4$	19.8	CH_4: 2.5vol%, GHSV: 20,000h^{-1}	409	491	70

1 M. Jeong, N. Nunotani, N. Moriyama and N. Imanaka, *Catal. Sci. Technol*., 2017, **7**, 1986.
2 S. Y. Kim, Y. B. Choi, T. W. Kang, J. H. Kim, D. Y. Kim, J. H. Jae, B. S. Bae and S. W. Kim, *Catal. Commun*., 2023, 178, 106670.
3 J. Lin, Y. Chen, J. Huang, G. Cai, Y. Xiao, Y. Zhan and Y. Zheng, *Int. J. Hydrogen Energy.*, 2021, **46**, 33397-33408.
4 M. J. Manto, P. Xie and C. Wang, *ACS Catal.*, 2017, **7**, 1931-1938.
5 A. Civera, G. Negro, S. Specchia, G. Saracco, V. Specchia, *Catal Today.*, 2005, **100(3–4)**, 275–81.
6 Y. Wang, H. Arandiyan, J. Scott, M. Aki, H. Dai, J. Deng, K. A. Zinsou and R. Amal, *ACS Catal.*, 2016, **6(10)**, 6935–47.
7 B. Kucharczyk, W. Tylus and L. Kpinski, *Appl. Catal. B.*, 2004, **49(1)**, 27–37.

8 G. Pecchi, P. Reyes, T. Lopez and R. Gomez, *J. Non-Cryst Solids.*, 2004, **345**, 624–7.
9 L. Xiao, K. Sun, X. Xu and X. Li, *Catal Commun.*, 2005, **6(12)**, 796–801.
10 C. Shi, L. Yang, J. Cai, *Fuel.*, 2007, **86(1–2)**, 106–12.
11 S. Specchia, P. Palmisano, E. Finocchio and G. Busca, *Chem. Eng. Sci.*, 2010, **65(1)**, 186–92.
12 Y.J. Zhang, J. R. Niu, G. Z. Wang, D. Li, H. X. Dai, H. He and W. G. Qiu, J. *Rare Earths.*, 2006, **24**, 1–5.
13 Z. X. Wu, J. G. Deng, Y. X. Liu, S. H. Xie, Y. Jiang, X. T. Zhao, J. Yang, H. Arandiyan, G. S. Guo and H. X. Dai, *J. Catal.*, 2015, **332**, 13–24.
14 P. Xu, Z. X. Wu, J. G. Deng, Y. X. Liu, S. H. Xie, G. S. Guo, H. X. Dai, *Chin. J. Catal.*, 2017, **38**, 92–105.
15 P. Xu, X. T. Zhao, X. Zhang, L. Bai, H. Q. Chang, Y. X. Liu, J. G. Deng, G. S. Guo and H. X. Dai, *Mol. Catal.*, 2017, **439**, 200–210.
16 X. Y. Li, Y. X. Liu, J. G. Deng, S. H. Xie, X. T. Zhao, Y. Zhang, K. F. Zhang, H. Arandiyan, G. S. Guo and H. X. Dai, *Appl. Surf. Sci.,* 2017, **403**, 590–600.

Table S2. Refined structural parameters of $Sr_3Fe_2O_7$ and $SrFeO_{2.75}$ obtained via Rietveld refinement of X-ray powder diffraction data acquired at room temperature

Refined structure parameters of $Sr_3Fe_2O_7$							Refined structure parameters of $SrFeO_{2.75}$						
Atom	Site	Occ.	x	y	z	Beq	Atom	Site	Occ.	x	y	z	Beq
Sr11	2b	1	0.00000	0.00000	0.50000	0.5	Sr21	2c	1	0.50000	0.00000	0.50000	0.5
Sr12	4e	1	0.00000	0.00000	0.31830	0.5	Sr22	2d	1	0.00000	0.00000	0.50000	0.5
Fe11	4e	1	0.00000	0.00000	0.10008	0.5	Sr23	4g	1	0.25600	0.00000	0.00000	0.5
O11	8g	1	0.00000	0.50000	0.09139	0.5	Fe21	4i	1	0.50000	0.24900	0.00000	0.5
O12	4e	1	0.00000	0.00000	0.20785	0.5	Fe22	4f	1	0.25000	0.25000	0.50000	0.5
O13	2a	1	0.00000	0.00000	0.00000	0.5	O21	2b	1	0.50000	0.00000	0.00000	0.5
							O22	4h	1	0.26600	0.00000	0.50000	0.5
							O23	16r	1	0.37900	0.26900	0.24700	0.5

Table S3. Composition of *a*wt%PdO/16wt%$Sr_3Fe_2O_{7-\delta}$/*a* –Al_2O_3 catalysts.

Sample	**Measured composition**
5wt%PdO/16wt%$Sr_3Fe_2O_{7-\delta}$/*a*–Al_2O_3	4.2wt%PdO/15.3wt%$Sr_3Fe_2O_{7-\delta}$/*a*–Al_2O_3
13wt%PdO/16wt%$Sr_3Fe_2O_{7-\delta}$/*a*–Al_2O_3	12.5wt%PdO/15.7wt%$Sr_3Fe_2O_{7-\delta}$/*a*–Al_2O_3
15wt% PdO/16wt%$Sr_3Fe_2O_{7-\delta}$/*a*–Al_2O_3	16.1wt% PdO/16.1wt%$Sr_3Fe_2O_{7-\delta}$/*a*–Al_2O_3
20wt% PdO/16wt%$Sr_3Fe_2O_{7-\delta}$/*a*–Al_2O_3	19.4wt% PdO/15.9wt%$Sr_3Fe_2O_{7-\delta}$/*a*–Al_2O_3

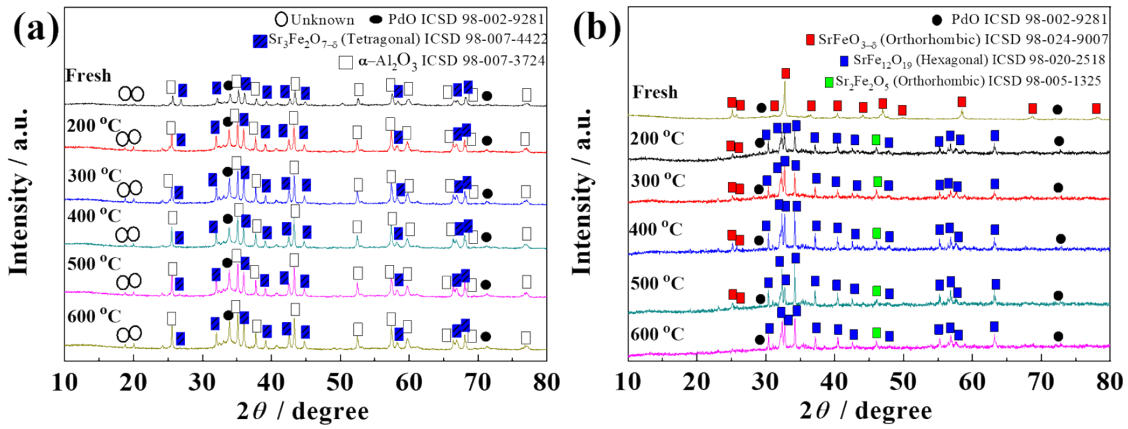

Figure S1. XRD pattern of (a) 10wt%PdO/16wt%$Sr_3Fe_2O_{7-\delta}$/α-Al_2O_3 and (b) 10wt%PdO/$SrFeO_{3-\delta}$ catalysts after thermal stability test at 200, 300, 400, 500, 600 ℃ for 1 h.

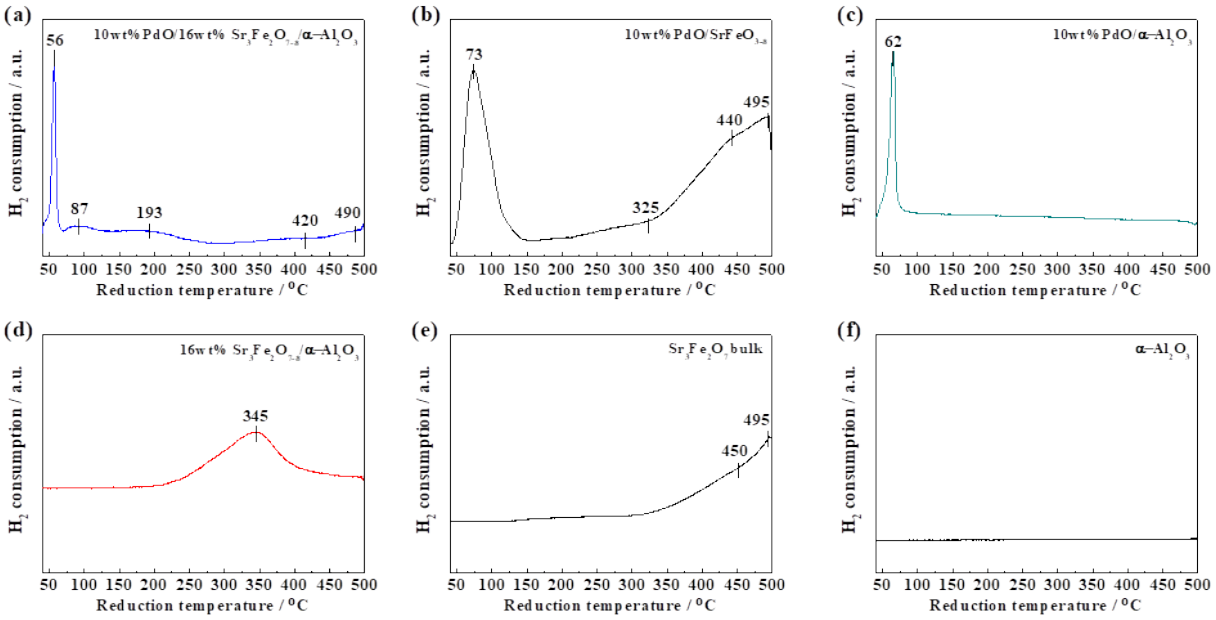

Figure S2. H_2-TPR profile for enlarged graph of (a) 10wt%PdO/16wt%$Sr_3Fe_2O_{7-\delta}$/α-Al_2O_3, (b) 10wt%PdO/$SrFeO_{3-\delta}$, (c) 10wt%PdO/α-Al_2O_3, (d) 16wt%$Sr_3Fe_2O_{7-\delta}$/α-Al_2O_3, (e) $Sr_3Fe_2O_7$ bulk, and (f) α-Al_2O_3.

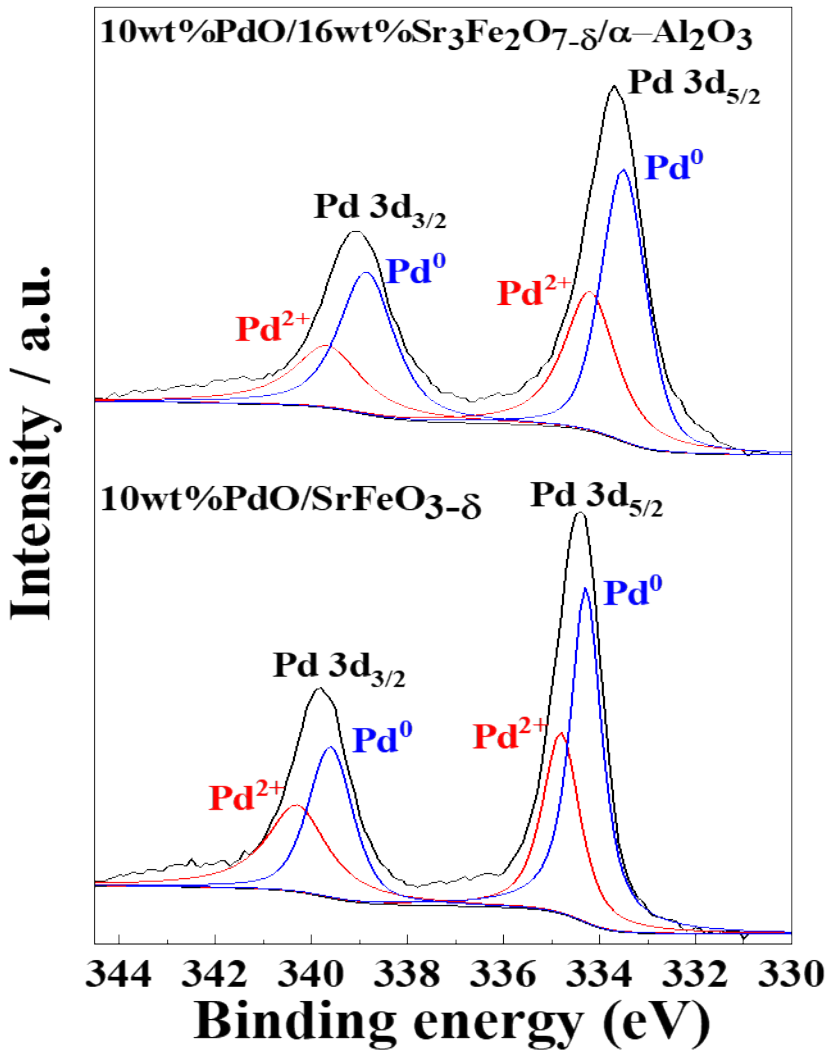

Figure S3. XPS spectra for Pd 3d core-level of 10wt%PdO/α-Al_2O_3, 10wt%PdO/$SrFeO_{3-\delta}$, and 10wt%PdO/16wt%$Sr_3Fe_2O_{7-\delta}$/α-Al_2O_3.

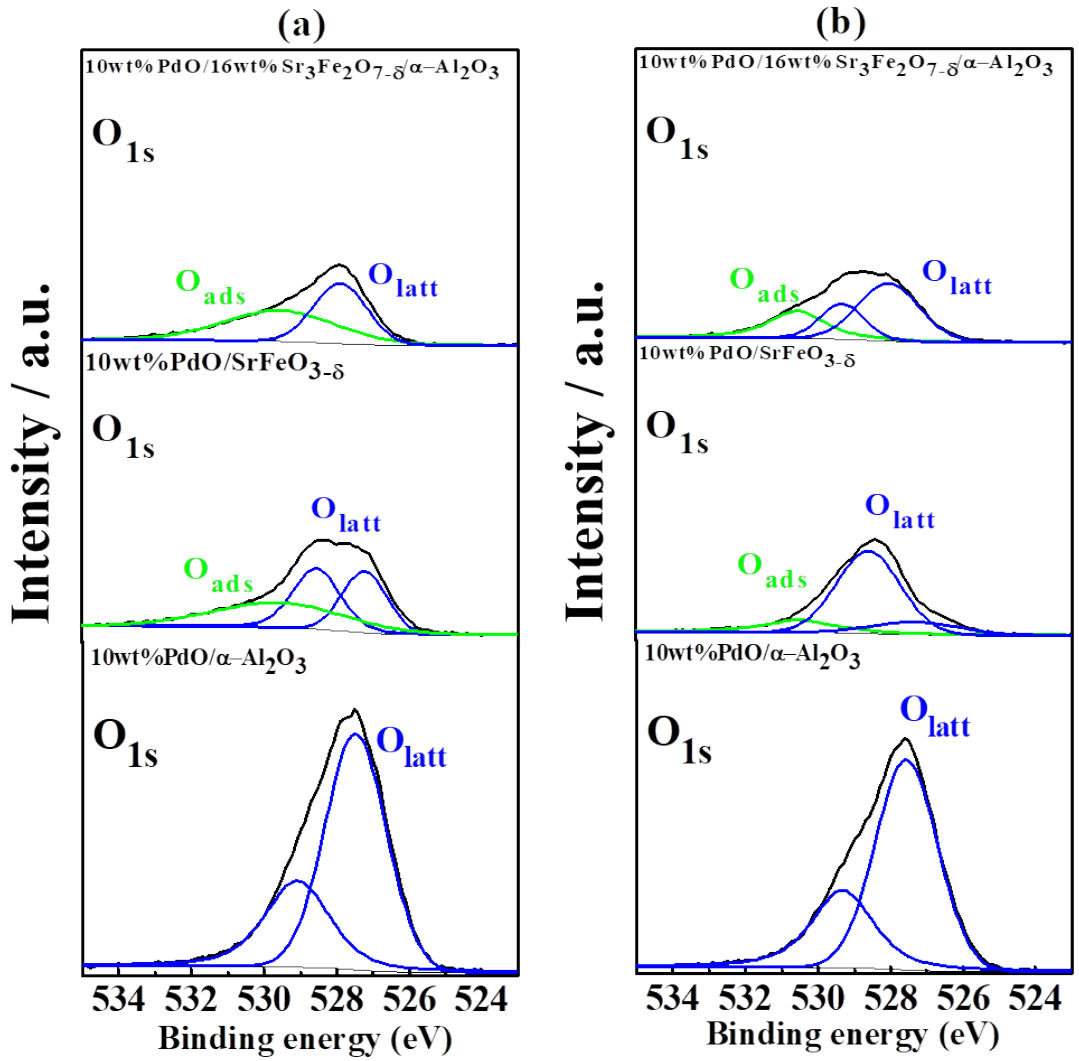

Figure S4. XPS spectra for O 1s core-level of 10wt%PdO/α-Al_2O_3, 10wt%PdO/$SrFeO_{3-\delta}$, and 10wt%PdO/16wt%$Sr_3Fe_2O_{7-\delta}$/α-Al_2O_3 before (a) and after (b) methane combustion reaction.

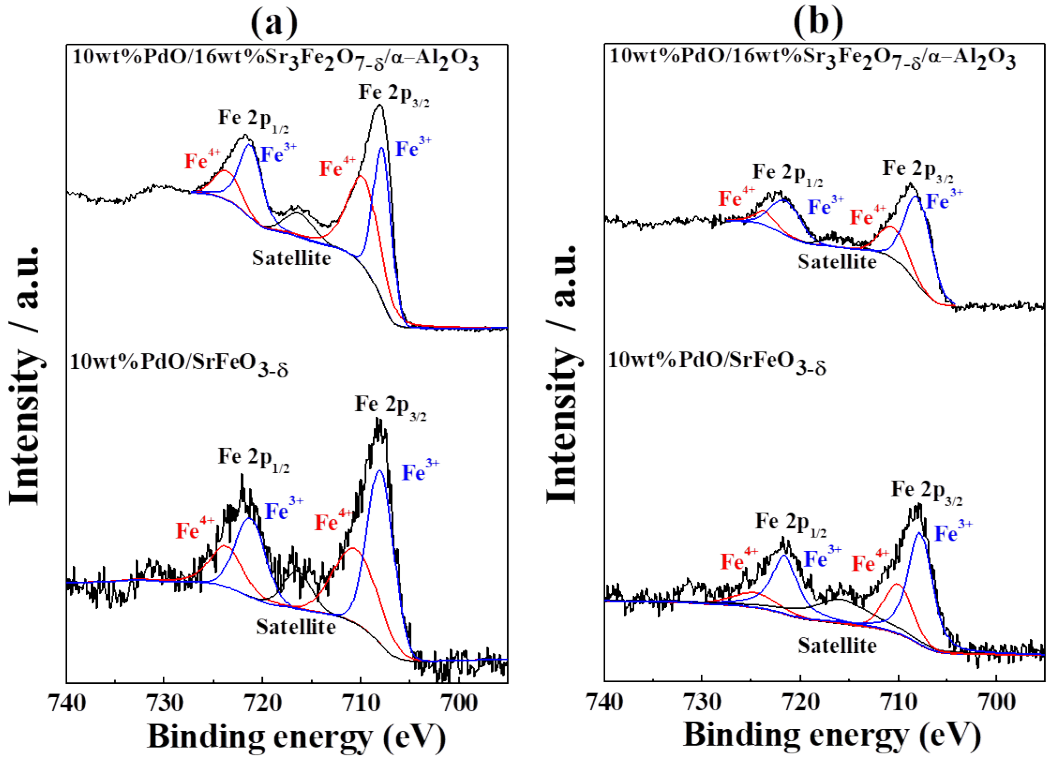

Figure S5. XPS spectra for Fe $2p_{3/2}$ and Fe $2p_{1/2}$ core-level of 10wt%PdO/α-Al_2O_3, 10wt%PdO/$SrFeO_{3-\delta}$, and 10wt%PdO/16wt%$Sr_3Fe_2O_{7-\delta}$/α-Al_2O_3 before (a) and after (b) methane combustion reaction.

Table S4. Surface atomic ratios of the before and after methane combustion reaction samples obtained from X-ray photoelectron spectrometer results and the values of PdO dispersion derived by the results of H_2-TPR and O_2-Pulse analyses.

Sample	PdO dispersion (%)	$Pd^{2+}/(Pd^{2+}+Pd^0)$ (%)	Oads/O (%)	Olatt/O (%)	Fe^{3+}/Fe (%)	Fe^{4+}/Fe (%)
10wt%PdO/16wt% $Sr_3Fe_2O_{7-\delta}$ /α-Al_2O_3 (before reaction)	7.69	40.31	53.67	46.32	58.98	41.01
10wt%PdO/16wt% $Sr_3Fe_2O_{7-\delta}$ /α-Al_2O_3 (after reaction)	-	-	28.65	71.35	73.11	26.89
10wt%PdO/$SrFeO_{3-\delta}$ (before reaction)	7.58	42.49	33.25	66.75	53.71	46.28
10wt%PdO/$SrFeO_{3-\delta}$ (after reaction)	-	-	16.66	83.33	70.67	29.33
10wt%PdO/α-Al_2O_3 (before reaction)	0.15	-	0	100	-	-
10wt%PdO/α-Al_2O_3 (after reaction)	-	-	0	100	-	-

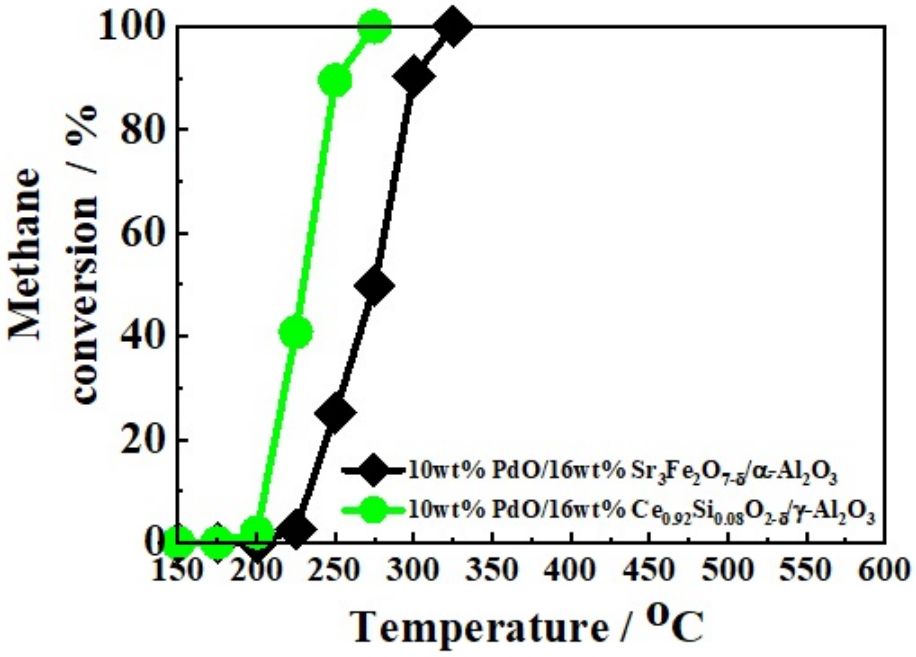

Figure S6. Temperature-dependence of methane oxidation over 10wt%PdO/16wt%$Ce_{0.92}Si_{0.08}O_{2-\delta}$/γ-$Al_2O_3$, and 10wt%PdO/16wt%$Sr_3Fe_2O_{7-\delta}$/α-$Al_2O_3$ catalysts.

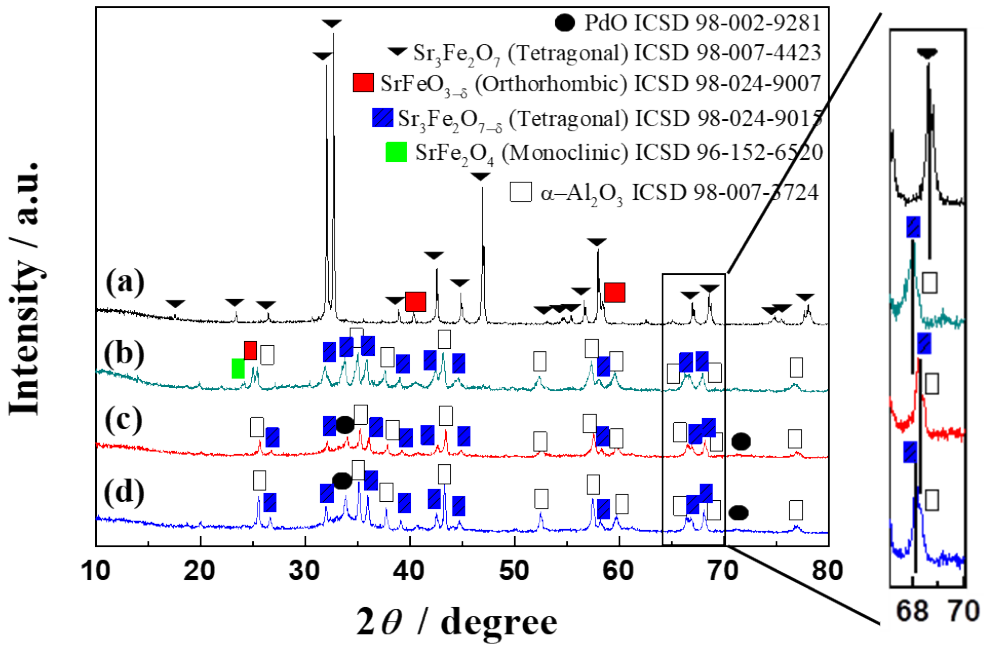

Figure S7. XRD pattern of (a) $Sr_3Fe_2O_7$, (b) 16wt%$Sr_3Fe_2O_{7-\delta}$/α-Al_2O_3, (c) 10wt%PdO/16wt%$Sr_3Fe_2O_{7-\delta}$/α-Al_2O_3 (before reaction), and (d) 10wt%PdO/16wt%$Sr_3Fe_2O_{7-\delta}$/α-Al_2O_3 (after reaction) catalysts.

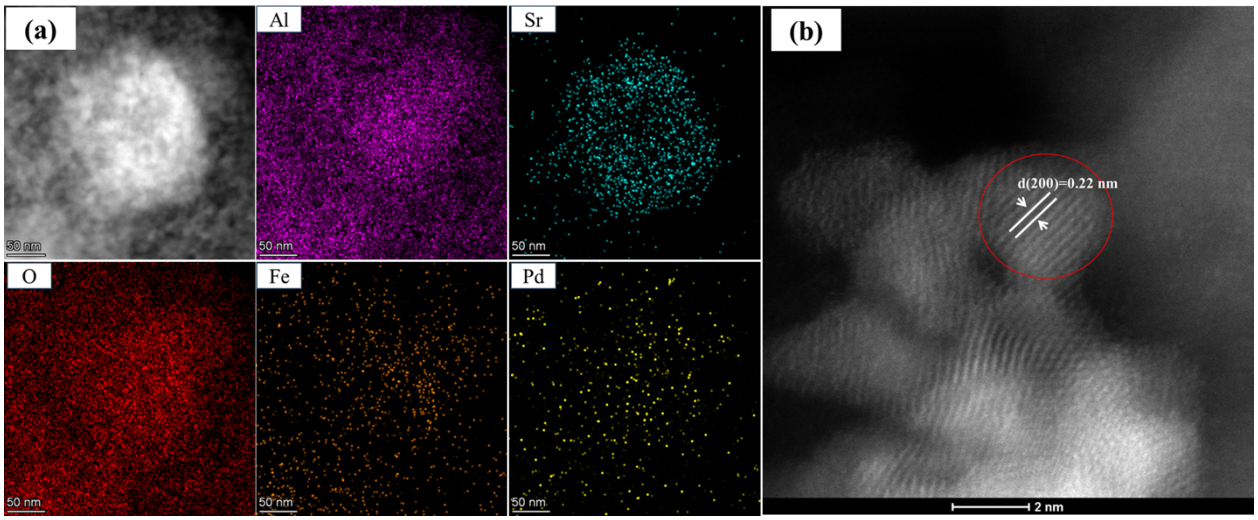

Figure S8. (a) EDS images and (b) high-resolution TEM image of the 13wt%PdO/16wt%$Sr_3Fe_2O_{7-\delta}$/α-Al_2O_3 catalysts.

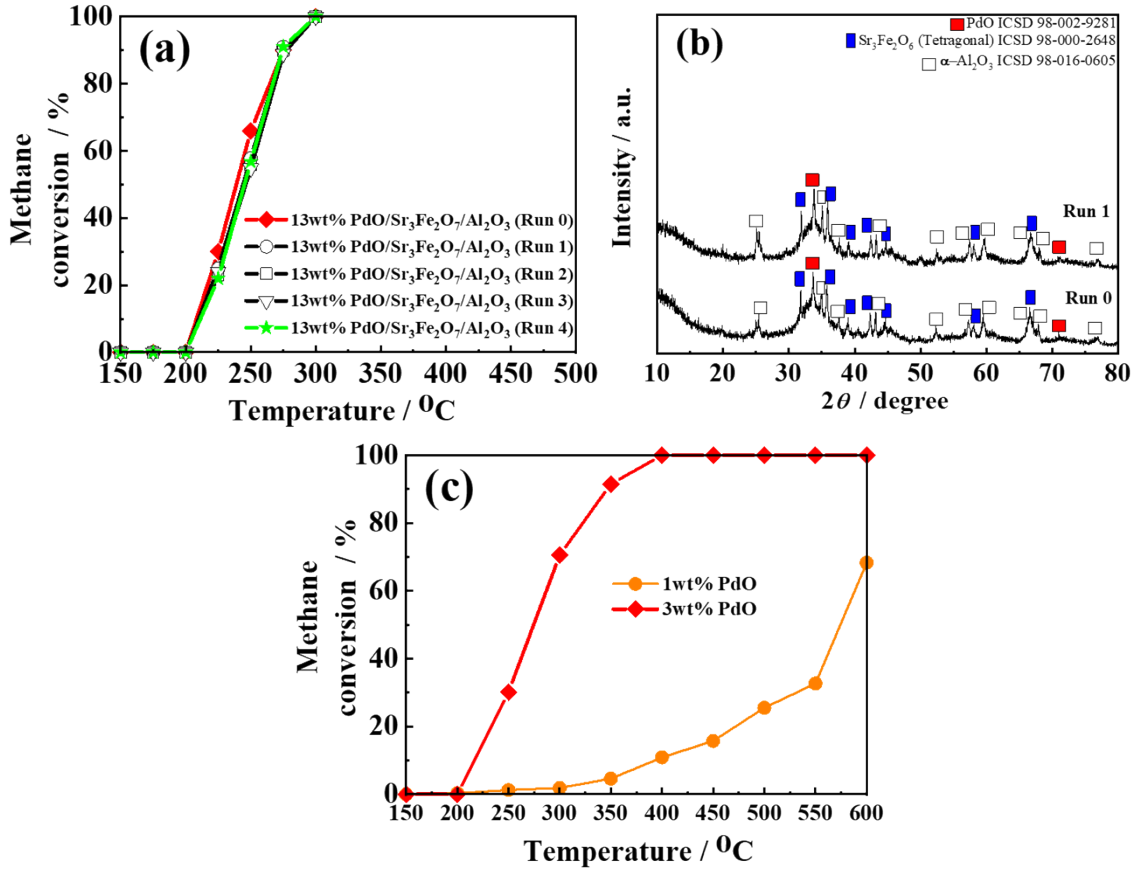

Figure S9. (a) Catalyst recycle test for methane combustion over the 13wt%PdO/16wt%$Sr_3Fe_2O_{7-\delta}$/α-Al_2O_3 catalysts, (b) XRD pattern of 13wt%PdO/16wt%$Sr_3Fe_2O_{7-\delta}$/α-Al_2O_3 catalysts after Run 0 and 1, and (c) Temperature-dependence of methane oxidation over αwt%PdO/16wt%$Sr_3Fe_2O_{7-\delta}$/α-Al_2O_3 catalysts (α = 1, 3) under the CH_4 concentration of 2.5% and mass hourly space velocity of 120,000 L·kg-^{1}·h^{-1}.